Supplementary Information (SI) for Nanoscale Horizons.

Detecting Conformational Changes in Switchable Heterodimer Plasmon Rulers through iSCAT Fluctuation Microscopy

Aidan Oi, Koustav Kundu, Ritesh K. Bag, Björn M. Reinhard
Department of Chemistry and The Photonics Center, Boston University,
Boston, MA 02215, United States

Supporting Information

Pairwise polarizability.

In this work we take established dipolar coupling approximation theory and extend it to an orientation dependent heterodimer model.[1] The dielectric function of gold was interpolated from Johnson and Christy's experimental work.[2] The following equations were used to simulate the heterodimer coupling with a quasistatic dipolar coupling model shown in **Figure 3**, where P is the polarization of each dipole, α, is the polarizability, and E_0 is the incident electric field in equations 1-3.[3] We then consider each dipole's response to the other's induced electric field in equations 4-6. G in equation 7 provides a scalar coupling constant of aligned dipoles (corresponding to the angular projection of the dyadic Green's function)[4] in NPs separated by distance d (center-to-center), and with ε_0 the permittivity of free space and ε_m the dielectric constant of the medium, which we will take as 1.77 in the case of room temperature water in the visible wavelength range.[5] Equation 8 show the total dipole moment with the pair polarizability, which is expressed in equation 9 using G from equation 7. In this expression α_1, and α_2 are polarizabilities of the individual NPs, that can be determined using the Clausius-Mossotti expression in

equation 10. The pairwise polarizability is then used in equations 12 and 13 to determine the wavelength-dependent scattering cross-section and phase plots shown in Figure 3, using equation 11 to calculate the wave vector through water.

$$P = \alpha E_0 \quad (1)$$

$$P_1 = \alpha_1(E_0 + GP_2) \quad (2)$$

$$P_2 = \alpha_2(E_0 + GP_1) \quad (3)$$

$$P_1 = \alpha_1\big(E_0 + G\alpha_2(E_0 + GP_1)\big) \quad (4)$$

$$P_1 = \frac{\alpha_1(E_0+G\alpha_2E_0)}{1-\alpha_1\alpha_2G^2} \quad (5)$$

$$P_2 = \frac{\alpha_2(E_0+G\alpha_1E_0)}{1-\alpha_1\alpha_2G^2} \quad (6)$$

$$E = GP\ with\ G = \frac{1}{4\pi\varepsilon_0\varepsilon_m d^3}(3cos^2(\theta) - 1) \quad (7)$$

$$P_{pair} = P_1 + P_2 = \alpha_{pair}E_0 \quad (8)$$

$$\alpha_{pair} = \frac{\alpha_1(1+G\alpha_2)}{1-\alpha_1\alpha_2G^2} + \frac{\alpha_2(1+G\alpha_1)}{1-\alpha_1\alpha_2G^2} = \frac{\alpha_1+\alpha_2+2G\alpha_1\alpha_2}{1-\alpha_1\alpha_2G^2} \quad (9)$$

$$\alpha_i = \varepsilon_0\varepsilon_m 4\pi {r_i}^3\left(\frac{\varepsilon_{Au}-\varepsilon_m}{\varepsilon_{Au}+2\varepsilon_m}\right) \quad (10)$$

$$k = 2\frac{\pi}{\lambda}\sqrt{\varepsilon_m} \quad (11)$$

$$\sigma = \frac{k^4}{6\pi{\varepsilon_0}^2}\left|\alpha_{pair}\right|^2 \quad (12)$$

$$\varphi = -i * \ln\left(\frac{\alpha_{pair}}{|\alpha_{pair}|}\right) \quad (13)$$

WLC model end-to-end length

The end-to-end distance of the DNA tether was calculated by independently calculating the $<R^2>$ values for each ssDNA or dsDNA segment using equation 14 and adding them together before taking the square root to determine <R> as shown in equation 15.[6]

$$< R^2 > = 2PL_0\left[1 - \frac{P}{L_0}\left(1 - e^{-L_0/P}\right)\right] \quad (14)$$

$$< R_{eff} > = \sqrt{< R_1{}^2 > + < R_2{}^2 > + < R_3{}^2 > + \cdots} \qquad (15)$$

Photothermal effect

The increase in temperature ΔT_{NP} for a 40 nm Au NP under our illumination conditions was evaluated as function absorption cross-section, σ_{abs}, the fluence of the incident electric-field, I_{inc}, the radius of the AuNP, R, and the thermal conductivity of water, κ_{water} using equation 16 below.[7] The fluence was determined by a power meter and irradiance was calculated to be approximately 3.4 kW/cm^2 in the confocal spot, which results in a ΔT_{NP} of 0.8 K for a 40 nm AuNP in our experimental setup. We expect that this ΔT_{NP} should have no relevant impact on our experimental data.

$$\Delta T_{NP} = \frac{\sigma_{abs} I_{inc}}{4\pi R \kappa_{water}} \qquad (16)$$

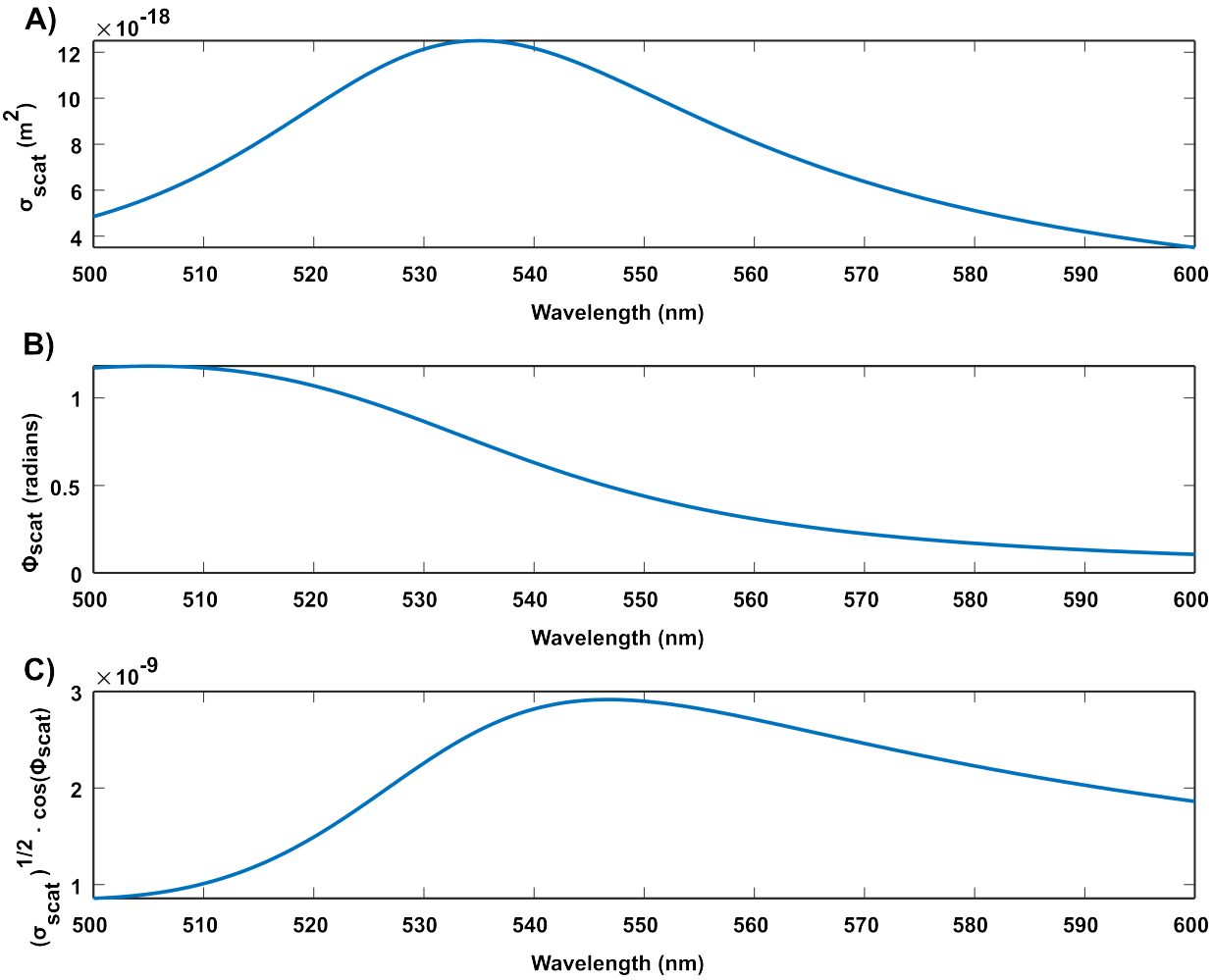

Figure S1: Simulated a) scattering cross-section σ_{scat} (~$|s|^2$), b) scattering phase ϕ_{scat}, and c) $\sqrt{\sigma_{scat}} * \cos(\phi scat)$ for a 20 nm Au NP

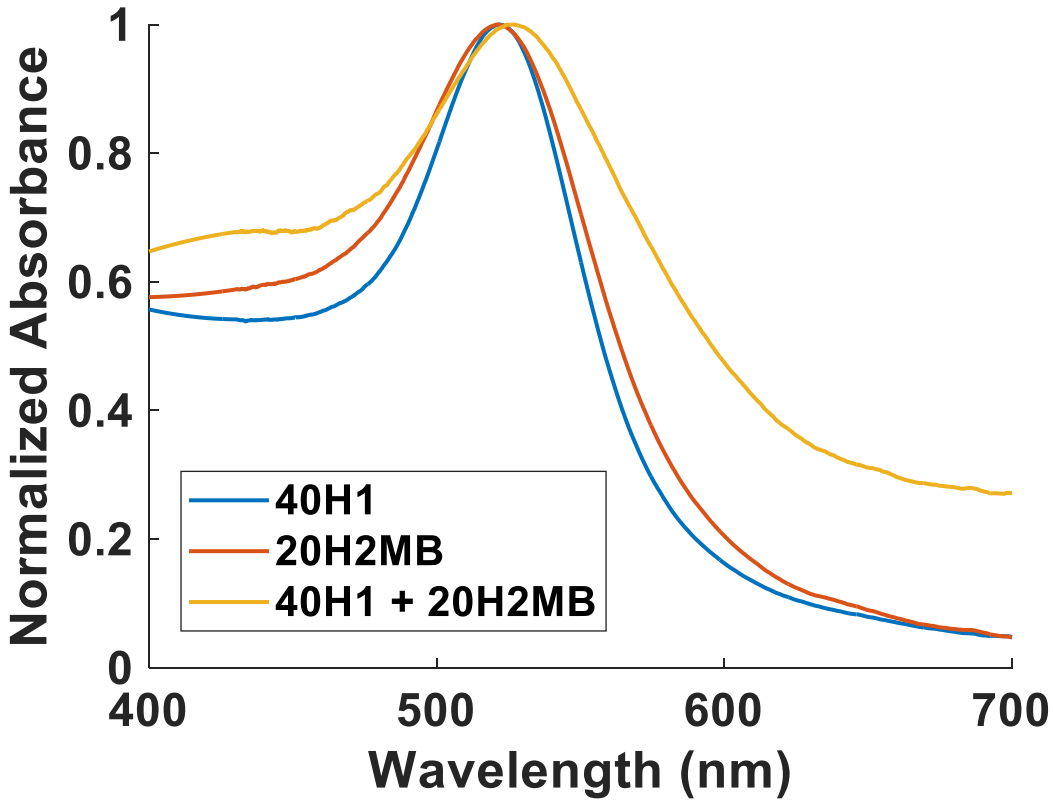

Figure S2: UV-VIS spectra of DNA-functionalized monomers (blue,red) and their annealed product (yellow). 40 nm Au NPs with handle H1 are labeled 40H1, 20 nm Au NPs with H2 and molecular beacon sequence is labeled as 20H2MB, and a mix of both particles is 40H1 + 20H2MB. A red-shift and broadening the peak in the annealed product is observed, indicating plasmon coupling in heterodimers and higher order aggregates.

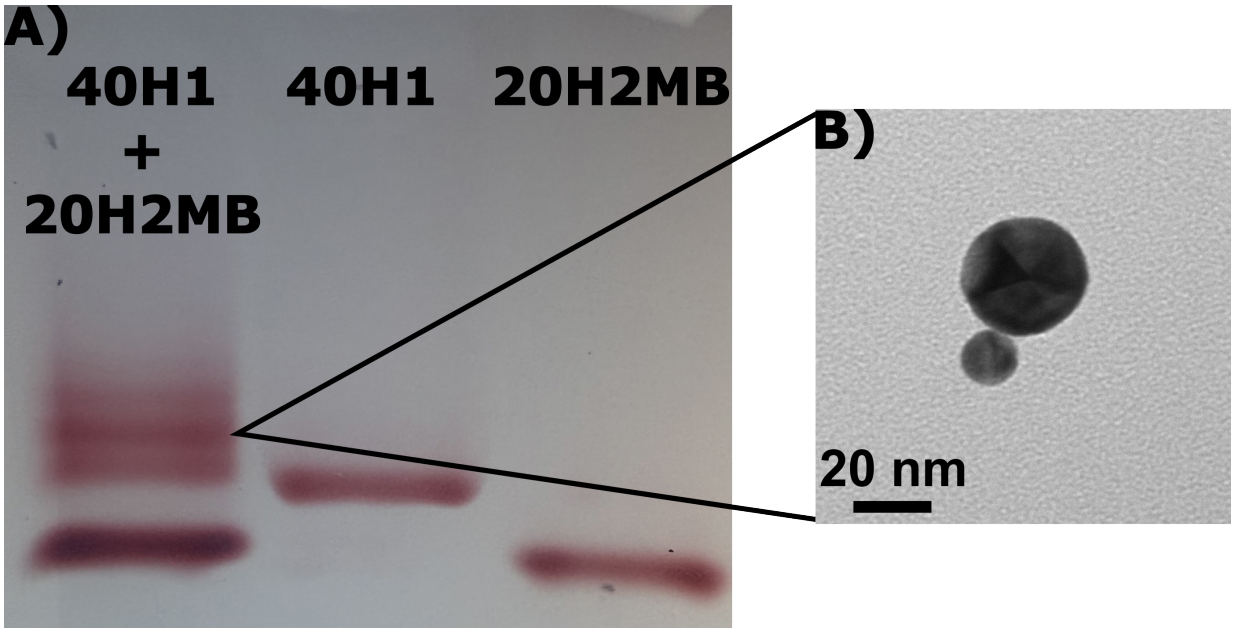

Figure S3: A) Gel image (1% agarose) of 40 nm and 20 nm Au NPs functionalized with complementary DNA as well as the annealed product. 40 nm Au NPs with handle H1 are labeled 40H1, 20 nm Au NPs with H2 and molecular beacon sequence is labeled as 20H2MB, and a mix of both particles is 40H1 + 20H2MB. The gel was run at 120V for 60min. B) Representative TEM image obtained from the excised dimer band from the gel. We frequently observed that under the high power of the TEM the dimer "collapsed" and the two NPs fused. We therefore primarily used SEM to characterize the NP assembly, as shown in Figure 1C,D in the main text.

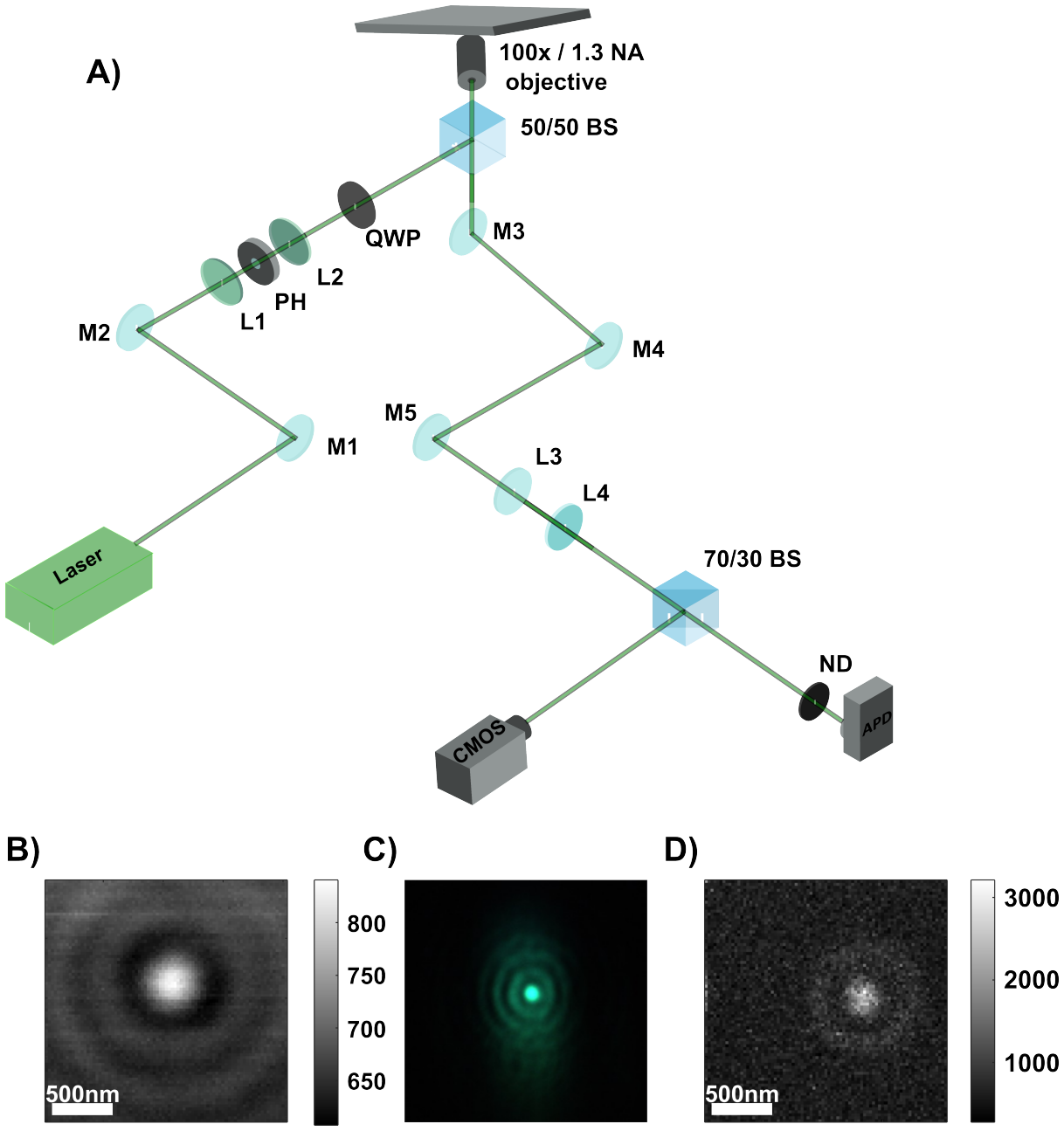

Figure S4: A) Scheme of experimental iSCAT setup. Abbreviations and specifications: BS, beamsplitter; M1-5, mirror; L1-4, lens (f = 5cm); QWP, quarter wave plate; CMOS, complementary metal oxide semiconductor; PDM, photodetector module; PH, 10µm pinhole. The 70/30 BS transmits 70% of the light to the PDM and reflects 30% to the CMOS; ND, neutral density filter (OD 1.5). Components used in this scheme are from Alexander Franzen's inkscape ComponentLibrary (2006). B) A representative image produced by raster scanning the surface of the sample around a monomer with 25 nm steps with the nano positioner and averaging 50 datapoints of 1 ms integration time collected with the PDM per position. C) A representative image of a heterodimer collected with a CMOS camera. D) A representative image of the signal variance (calculated from 50 datapoints of 1ms integration time) of the heterodimer signal collected by PDM by raster scanning the sample in 25 nm steps with the nano positioner.

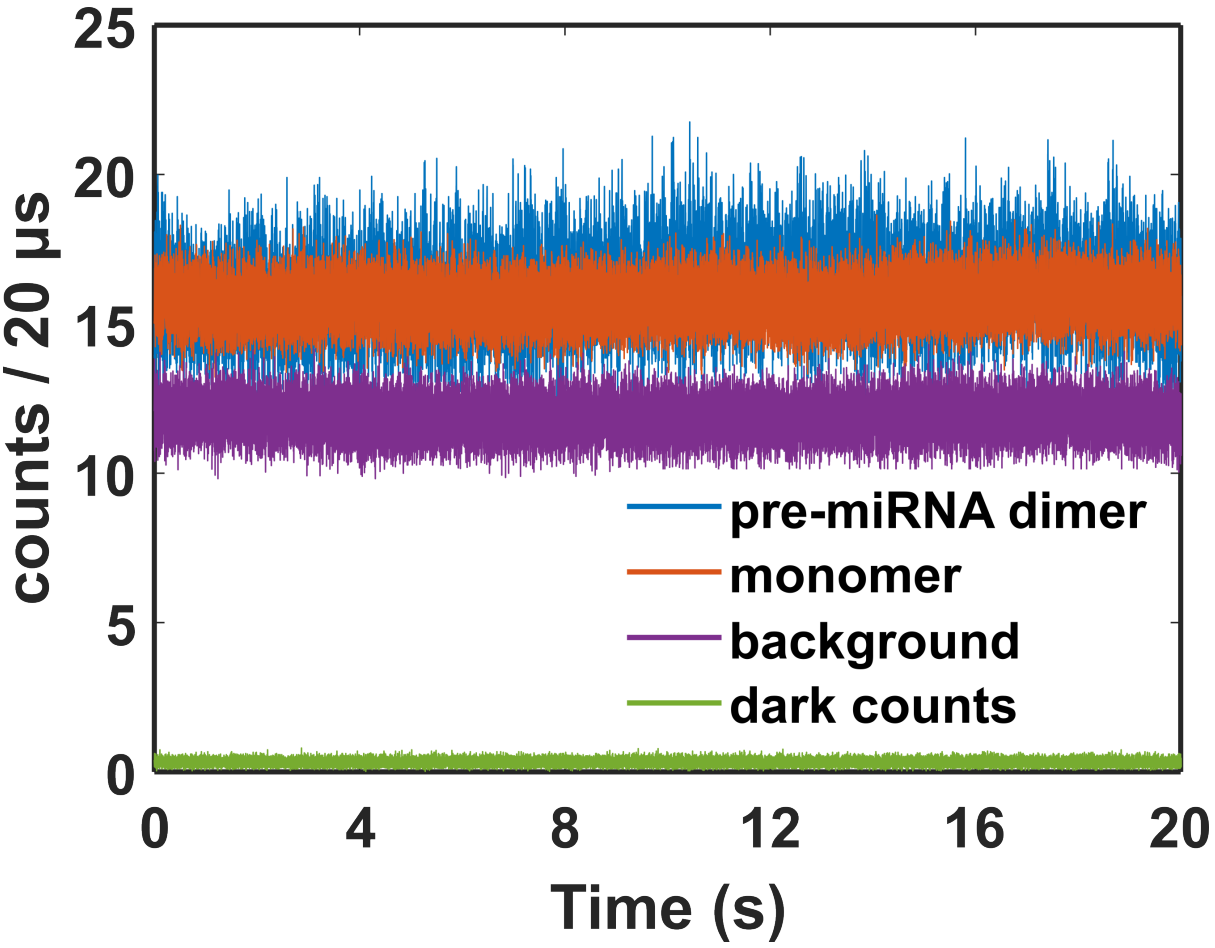

Figure S5: Raw PDM counts with 20 microsecond integration time and 50-point sliding average for various representative trajectories.

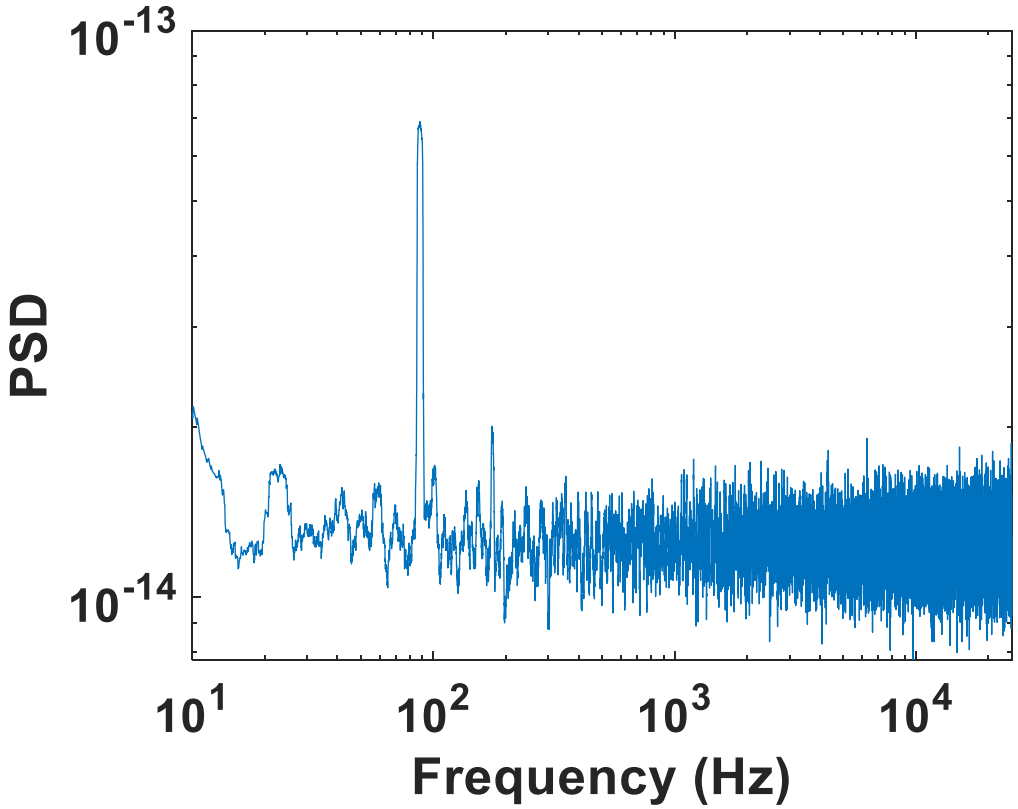

Figure S6: single dimer PSD plot post-spermidine (100-point sliding average). The pronounced feature at ~90 Hz indicates an experimental artifact.

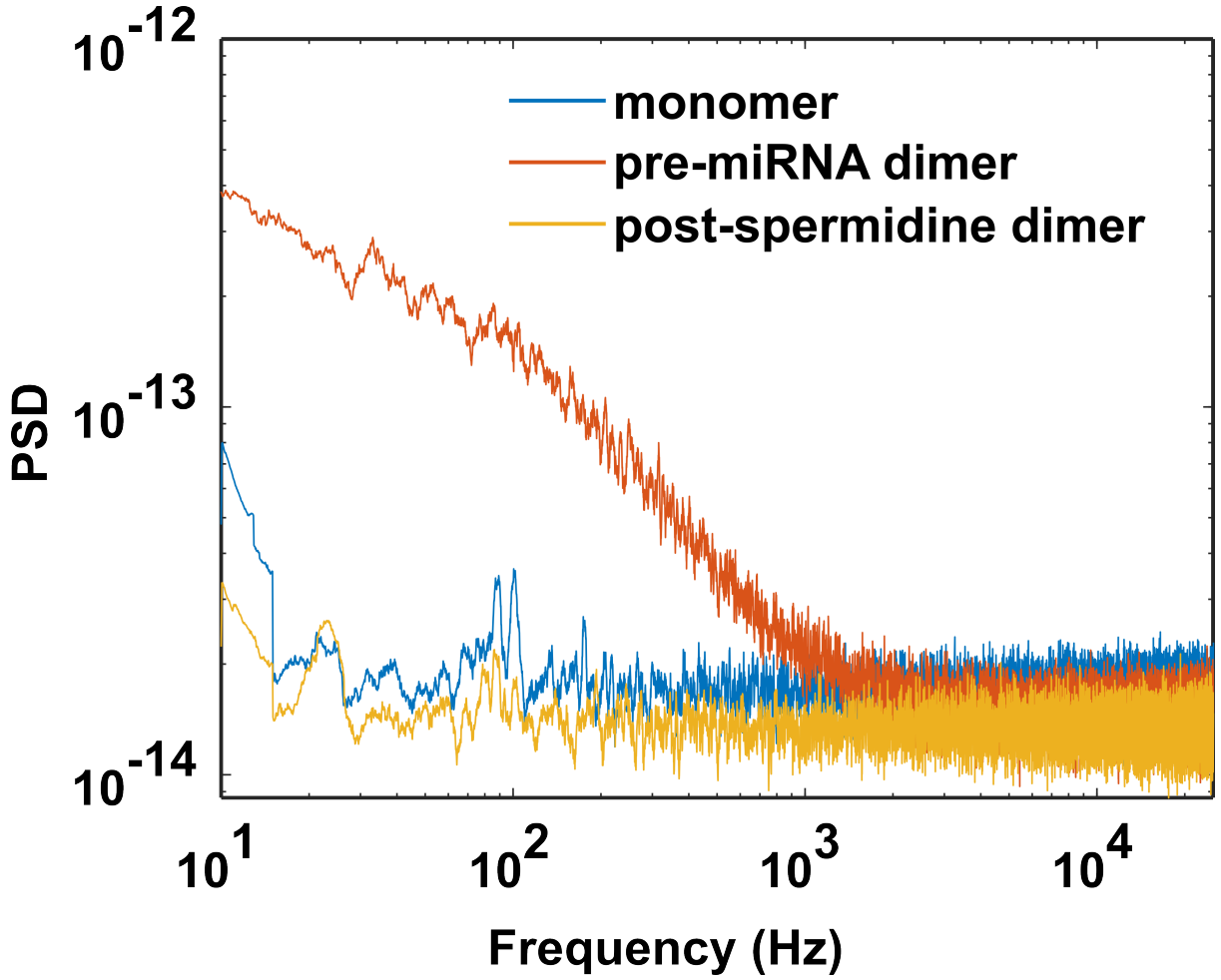

Figure S7: Power spectral density plots of a representative monomer (blue), pre-miRNA dimer (red), and the same dimer post-spermidine (yellow) with a 100-point sliding average.

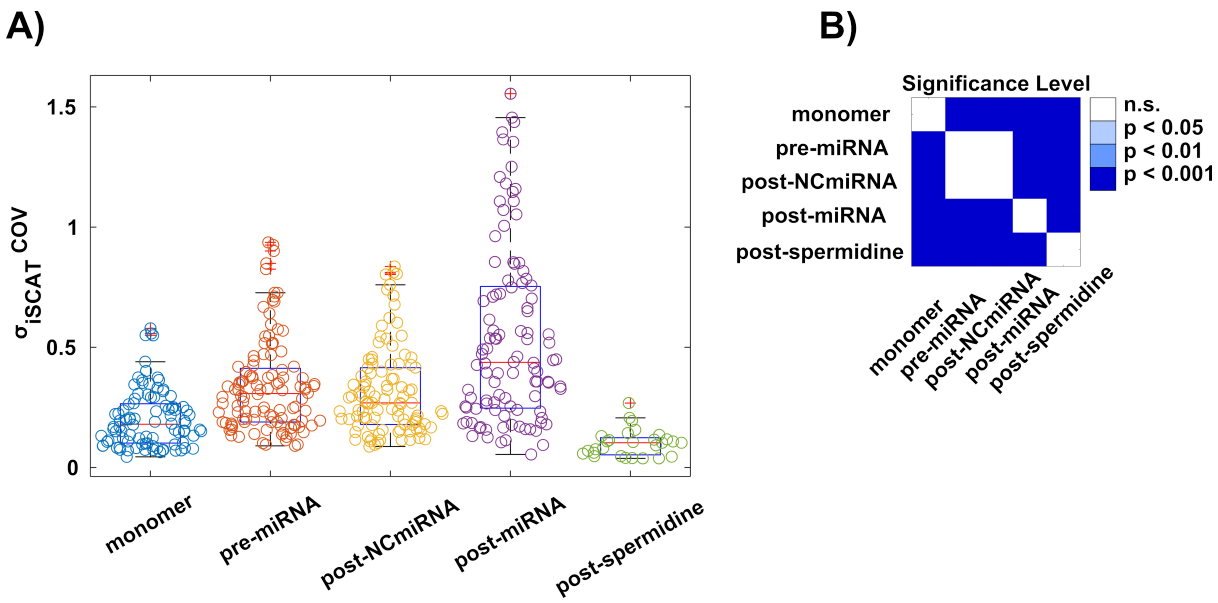

Figure S8: Comparison of the coefficient of variance (COV) for iSCAT contrast σ_{iSCAT} for 40 nm / 20 nm AuNP heterodimers under specified conditions, as well for 40nm AuNP monomers. The number of trajectories for each condition after removing outliers that deviate more than three scaled MAD from the median is (from left to right): 92, 112, 103, 104, 28. The heterodimer data was collected from at least five different batches.

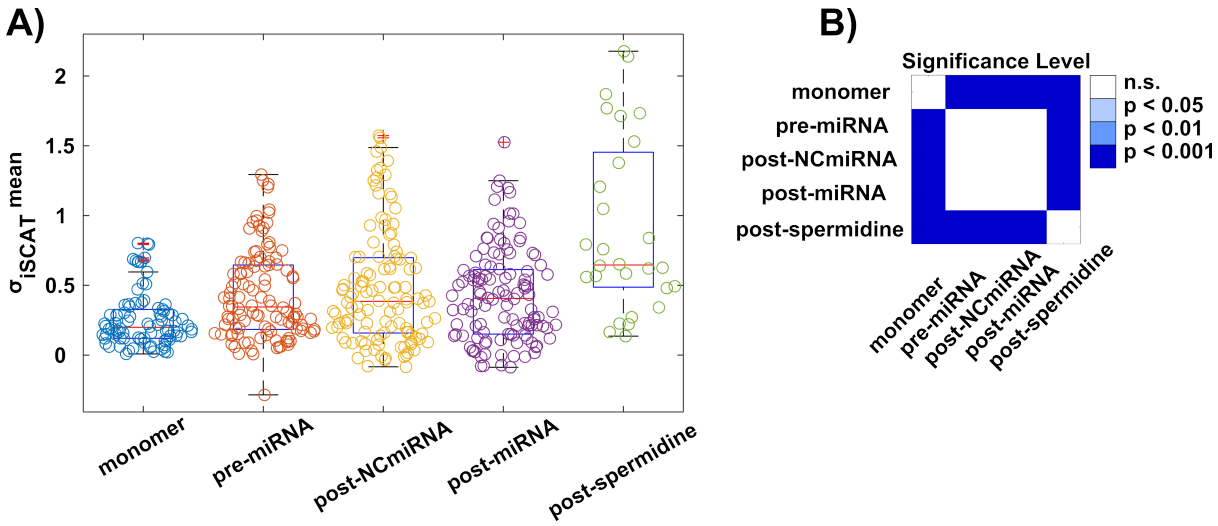

Figure S9: A) Comparison of the mean iSCAT contrast for 40 nm / 20 nm AuNP heterodimers under specified conditions, as well for 40nm AuNP monomers. The number of trajectories for each condition after removing outliers that deviate more than three scaled MAD from the median is (from left to right): 86, 114, 117, 120, 28. The heterodimer data was collected from at least five different batches. B) P-value heatmap for a two-tailed Student's t-test.

Table S1. Dimer assembly DLS data

	40 BSPP	20 BSPP	40H1	20H2	20H2MB	40H1+20H2 MB
Z-Average (nm)	41.0	19.9	47.5	25.3	27.0	117.4
Standard Deviation (nm)	0.9	0.7	0.2	0.4	0.6	4.2
Polydispersion Index (PDI)	0.1	0.1	0.1	0.2	0.1	0.3

40: 40 nm Au NP
20: 20 nm Au NP
H1: Handle 1
H2: Handle 2
MB: Molecular Beacon sequence

(1) Bohren, C. F.; Huffman, D. R. *Absorption and Scattering of Light by Small Particles*, 1st ed.; Wiley, 1998. https://doi.org/10.1002/9783527618156.

(2) Johnson, P. B.; Christy, R. W. Optical Constants of the Noble Metals. *Phys. Rev. B* **1972**, *6* (12), 4370–4379. https://doi.org/10.1103/PhysRevB.6.4370.

(3) Draine, B. T.; Goodman, J. Beyond Clausius-Mossotti - Wave Propagation on a Polarizable Point Lattice and the Discrete Dipole Approximation. *ApJ* **1993**, *405*, 685. https://doi.org/10.1086/172396.

(4) Jackson, J. D. *Classical Electrodynamics*, 3rd ed.; Wiley: New York, 1999.

(5) Hale, G. M.; Querry, M. R. Optical Constants of Water in the 200-Nm to 200-Mm Wavelength Region. *Appl. Opt.* **1973**, *12* (3), 555. https://doi.org/10.1364/ao.12.000555.

(6) Worm-Like Chain (WLC) Model. In *Encyclopedia of Biophysics*; Springer Berlin Heidelberg: Berlin, Heidelberg, 2013; pp 2757–2760. https://doi.org/10.1007/978-3-642-16712-6_502.

(7) Baffou, G.; Quidant, R. Thermo-plasmonics: Using Metallic Nanostructures as Nano-sources of Heat. *Laser & Photonics Reviews* **2013**, *7* (2), 171–187. https://doi.org/10.1002/lpor.201200003.